The International Journal of Advanced Manufacturing Technology (2020) 111:3241–3257
https://doi.org/10.1007/s00170-020-06320-8

ORIGINAL ARTICLE

Experimental investigations and its dimensional analysis–based modeling of the UAECDM process

Ranjeet Singh Rathore [1] · Akshay Dvivedi [1]

Received: 23 May 2020 / Accepted: 28 October 2020 / Published online: 9 November 2020

Abstract

The ultrasonic-assisted electrochemical discharge machining (UAECDM) process uses thermal, chemical, and ultrasonic energy together during the machining process. The energy produced from the discharge is used in the work material to produce micro-feature, but the entire energy is not used solely for material removal. Hence, it also affects the tool electrode wear (TEW) along with the material removal rate (MRR). An attempt has been made in this article to investigate the effect of process parameters related to the UAECDM process performance. From the experimental results, it was found that the ultrasonic vibrational amplitude influences the MRR and TEW most compared to other process parameters such as pulse on time (T_{on}), electrolyte concentration, and applied voltage. In addition, mathematical models are developed using dimensional analysis to predict TEW and MRR. It is based on process parameters affecting TEW and MRR, including the tool electrode and work material's thermal-physical properties. The results obtained from the mathematical models are quite similar to experimental results, and it has been found that the models can be used for further process's effects on performance characteristics.

Keywords Dimensional analysis · MRR · Modeling · TEW · UAECDM

1 Introduction

Ultrasound is a physical wave that propagates at frequencies higher than 20 kHz, i.e., above the human audible sound. Hence, it is suitable for various applications, namely medical, joining, and machining. Ultrasonic vibrations are provided to machine hard and brittle materials as direct input in the machining process, such as the ultrasonic machining (USM) process. As shown in Fig. 1, the USM facility comprises an ultrasonic generator, transducer, and horn. These units are coupled in sequence to provide high amplitude at the horn end. The tool is mounted at the horn end to utilize the maximum vibrational energy for the machining. The power intensity that passes through the cross-sectional area of the tool depends on both ultrasonic frequency and amplitude. But, high aspect ratio is difficult to reach during the USM process and is usually associated with low MRR [1, 2].

Ultrasonic vibrations can also be used to assist various conventional and non-conventional processes during machining. The literature reveals that the integration of ultrasonic vibrations with conventional machining reduces the forces required, and also increases the product quality. Pujana et al. investigated the ultrasonic vibration's effect during the machining in Ti6Al4V alloy. During the ultrasonic-assisted drilling (UAD) process, the same chip geometry was observed with the formation of the null burr. Due to the strain-softening effect, the feed forces decreased by 10–20%. The temperature at the tooltip, however, increases compared to traditional drilling [3]. During the ultrasonic-assisted milling process, Ni et al. developed an analytical model for evaluating the contact rate between tool and work material. It was observed that the cutting forces decreased by 35% due to the intermittent cutting effect. Surface quality of the finished product also improved during machining of the Ti6Al4V alloy [4]. Lofti et al. analyzed the ultrasonic vibration's effect in the tool chip contact friction by simulation and experimentation. It was found that the coefficient of friction and contact length decreases due to intermittent contact of the vibrated tool because of the thermal conduction time reduced at the interface of the tool chips [5].

✉ Ranjeet Singh Rathore
rathorers2001@gmail.com

Akshay Dvivedi
akshaydvivedi@gmail.com

[1] Mechanical and Industrial Engineering Department, Indian Institute of Technology Roorkee, Roorkee 247667, India

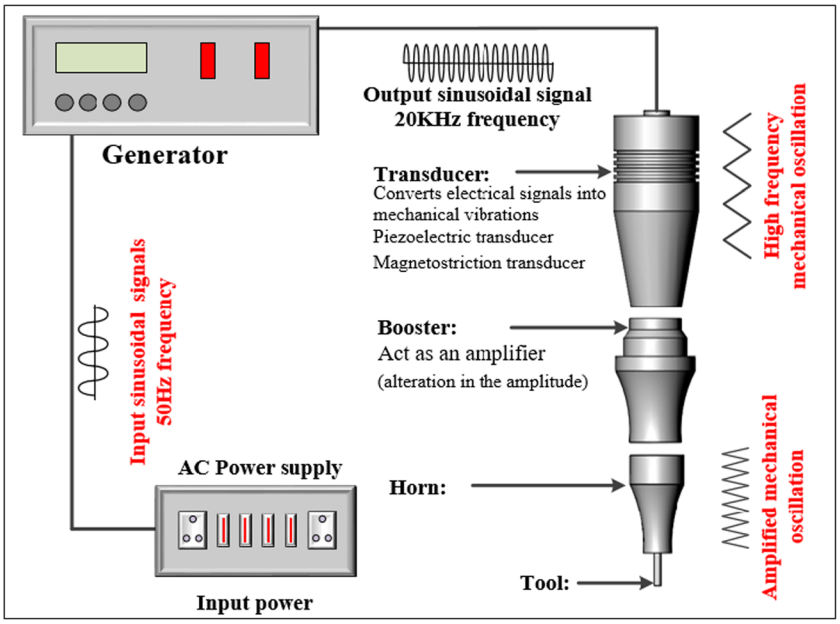

Fig. 1 Schematics of various components of the ultrasonic facility

Ultrasonic vibrations can also be used for performance improvement of various non-conventional machining processes. Kremer et al. introduced the concept of ultrasonic vibrations in the electric discharge machining (EDM) process to enhance slurry circulation and debris evacuation from the machining zone by high-frequency pumping action [6]. Yue et al. developed a FEM-based theoretical model to predict drilled hole profile and heat-effected zone boundary, and recast layer thickness for with and without ultrasonic-assisted laser. Deeper holes with minimal recast layer could be drilled with ultrasonic laser-assisted (USL) because the molten metal pressure and flow velocity are high, and the vapor point of the material has been modified [7]. During the ECDM process, Han et al. provided the electrolyte with ultrasonic vibrations to enhance the process performance. It was found that machining depth increased due to adequate electrolyte flow in the working gap, which provides gas film stability and improves the drilled hole surface quality [8]. It has been found from the literature that with the assistance of sonication, the performance of both conventional and non-conventional machining processes enhances.

The ECDM process is a hybrid non-conventional machining process to machine hard and brittle material [9]. It utilizes the thermal as well as chemical energy during the process [10, 11]. Thermal energy is produced at the tooltip due to breakdown of gas film formed during electrolysis, and chemical energy is generated by the flow of ions in an alkali electrolyte solution [12]. During the ECDM process, the tool electrode is immersed, and both anode and work materials are submerged in the electrolytic solution (Fig. 3a). The electrolysis process begins when the pulsed DC power supply is connected to the terminal of both the electrodes [13]. The generation, nucleation, and gas bubbles departure occur during the electrolysis process. The coalescence of these gas bubbles begins to form a film of gas over the surface of the tool electrode [14]. Due to the breaking down of gas film around the periphery of the tool electrode, the sparks initiate [15]. These discharges produced high thermal energy in the working gap, which melts and evaporates the work material [16]. A certain amount of energy produced is also transferred to the tool electrode, which affects the shape and size of the tool electrode, which refers to the TEW. It is interesting to note that the process performance of the ultrasonic-assisted electrochemical discharge machining (UAECDM) process is improved by controlling the discharge energy. Elhami et al. observed that, due to electrolyte replenishment from the working gap, the output performance increases with the sonicated tool electrode in the ECDM process. The surface cracks with low material removal rate (MRR) was found at a high amplitude of vibration due to large and dense current pulse generation at the hole entrance [17]. Rathore et al. introduced the sonicated tool electrode to enhance response characteristics during the ECDM process at higher applied voltage. It has been reported that the MRR increases, and the HOC decreases during the UAECDM process due to the reduction in thickness of gas film [18]. There are only a few publications available for the UAECDM process. The UAECDM process is still under investigation.

Modeling is a powerful tool that offers a way to understand the effects on the output characteristics of various input process parameters [19–21]. Various researchers have used the Buckingham π theorem to model MRR, surface roughness, etc. during different machining processes. Tsai et al. developed a semi-empirical model using the Buckingham π theorem to establish the relationship between work material surface finish and various process parameters during the EDM process [22]. Kumar et al. used the Buckingham theorem to

develop a model for evaluating the influence of process parameters on TEW during machining of titanium by USM [23]. Patil et al. developed a mathematical model for the determination of MRR of metal matrix composites during wire-EDM using dimensional analysis [24]. A mathematical model is developed to investigate the hot chamber die casting surface hardness using the Buckingham π theorem by Singh [25]. Singh and Singh developed a wear model based on the dimensional analysis for functionally graded material by fusion deposition modeling [26]. Bains et al. investigated the magnetic field effect during metal matrix composite (MMC) machining in the EDM process and established a relationship between process parameters using the Buckingham π theorem [27]. Goel et al. employed the Buckingham's π theorem to model the MRR and hole taper for the UA-jet electrochemical microdrilling process. These models are validated with the experimental results and found a good agreement with the statistical models [28]. A predictive model using the Buckingham π theorem is developed by Reddy et al. to predict the MRR during the machining of Hastelloy C276 by the EDM process [29]. Phate et al. predicted the surface quality of the aluminum-based alloy during the EDM process by using dimensional exponential model (Buckingham π theorem) [30]. Using the Buckingham's π theorem, Mohankumar et al. developed a semi-empirical model to predict the depth of cut of metal MMCs during AWJM and is compared to the regression model and experimental results [31]. The Buckingham π theorem has been found to be applied to solve various engineering problems and was found to be effective. Hence, this technique is suitable for TEW and MRR modeling during the UAECDM process.

Information about the influence of ultrasonic vibrations is not yet revealed during the ECDM process at higher applied voltage. Aside from that, any information about the mathematical modeling of TEW does not reveal in the literature. Therefore, mathematical models need to be developed, covering all performance aspects of the ECDM process as well as TEW in a holistic way. This investigation aims to evaluate the output response (MRR and TEW) as well as develop their mathematical models too. Experimental results have also concurred with the established models. The TEW model is validated with the experimental results with the stainless steel tool electrode, and these models also stand for other materials. The universal models are developed for the TEW and are in line with the results reported [32].

2 Materials and methods

2.1 Experimental design

2.1.1 Ultrasonic-assisted electrochemical discharge machining process description

Figures 2 and 3 show the schematic and photographic view of the indigenous UAECDM facility developed in the Advanced Manufacturing Laboratory at IIT, Roorkee. The UAECDM process is the hybrid of electrochemical machining (ECM), EDM, and USM processes. It utilizes the vibrational energy along with thermal and chemical energy. The assistance of ultrasonic vibration with the ECDM process requires equipment such as the ultrasosnic generator, transducer, and horn, which generate ultrasonic vibrations. The ultrasonic generator transforms low-frequency electrical signals into an electrical signal of high frequency. Such electrical high-frequency signals are fed to the piezoelectric transducer, which transforms electrical signals into mechanical vibrations. These vibrations are amplified with the energy-focusing device horn. The tool

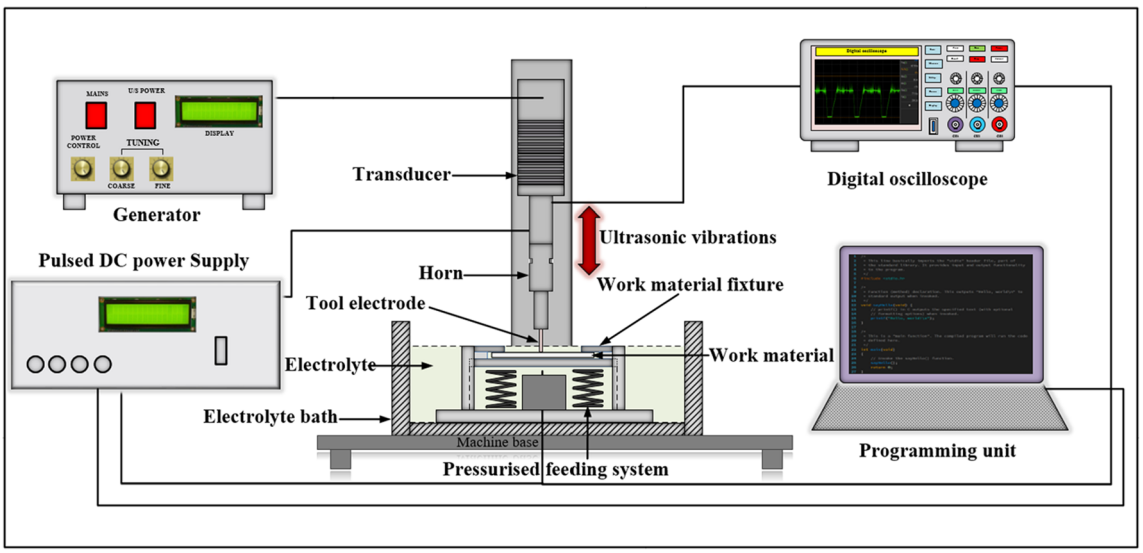

Fig. 2 Schematics of the UAECDM facility

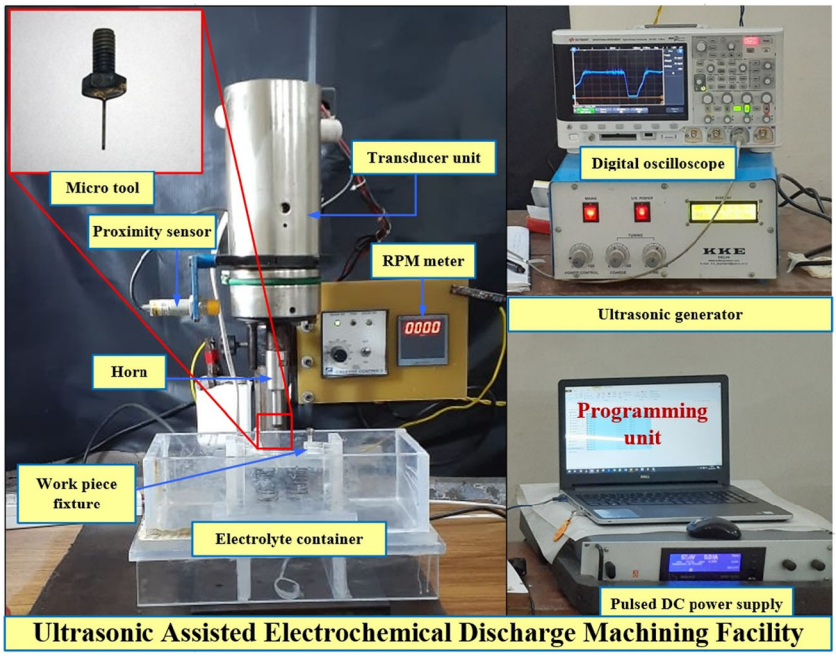

Fig. 3 Photographic view of the UAECDM facility

electrode is mounted to the horn end, which leads tool electrode to vibrate at high frequency (26.4 kHz) along the longitudinal axis. The tool electrode vibrations affect the departure radius of the gas bubble during the electrolysis process, which controls the formation of the gas film. During the process, the formation of thin gas film produces high-intensity and high-frequency discharges and results in material removal from the work material [33].

2.1.2 Material removal mechanisms during the UAECDM process

The UAECDM process is a hybridization of three non-conventional machining processes (ECM, EDM, USM). This hybrid process has taken advantage of various energy utilization, i.e., chemical energy, thermal energy, and mechanical energy simultaneously for drilling microholes in the work material. Figure 4 shows the schematics of ECDM and UAECDM process mechanisms. During the ECDM process, the pulsed DC power supply is applied across the tool electrode and auxiliary counter electrode, which initiates the electrolysis process and results in the generation of large-sized hydrogen gas bubbles from the tool electrode as shown in Fig. 4b. These large size gas bubbles come closer to each other, and the coalescence process takes place, which results in the formation of the thick gas film around the tool electrode, as shown in Fig. 4c. Due to the availability of potential above the critical voltage, the breakdown of insulated gas film takes place and results in the generation of high-intensity and low-frequency sparks, as shown in Fig. 4d. These sparks remove

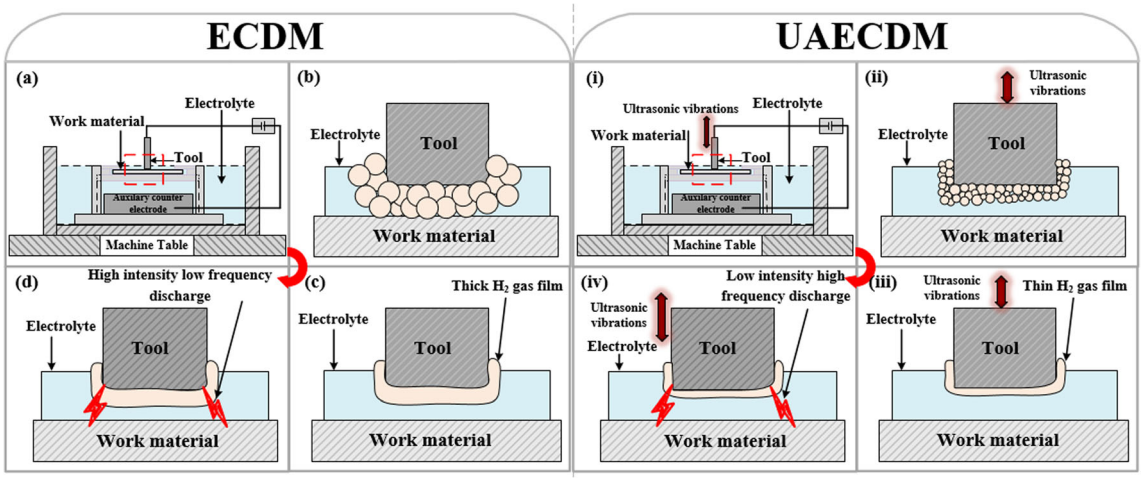

Fig. 4 Schematics for the ECDM and UAECDM process mechanism

the material from the work material by melting and evaporation, chemical etching, and thermal erosion. In the UAECDM process, the process mechanism changed with the introduction of ultrasonic vibrations to the tool electrode. The translatory motion of the tool electrode changes the dynamics of the gas bubble generation. The gas bubble departure radius decreases with the introduction of ultrasonic vibrations to the tool electrode, which results in the generation of small-sized gas bubbles around the tool electrode, as shown in Fig. 4(ii) [18]. These small size gas bubbles coalesce with each other, which results in the formation of the thin gas film around the tool electrode (Fig. 4(iii)). Besides that, an ultrasonically vibrated tool flatten the gas bubbles beneath the tool electrode that results in the extra thinning of the gas film. Figure 4 (iv) shows that there is a generation of high-frequency and low-intensity sparks with the breakdown of thin gas film that increases the quality characteristics of the drilled microholes.

2.1.3 Process conditions during the experiments

The process parameters that affect the MRR and TEW during the UAECDM process are T_{on}, applied voltage, power rating, and electrolyte concentration. The cause and effect diagram for the MRR and TEW in the UAECDM process is based on the literature, as shown in Fig. 5.

The effect of process parameters can be independently analyzed depending on the properties of the tool characteristics, the work material, and the operating parameters, as given in Table 3. The relation between the power rating and amplitude is given in Table 4. In this article, the stainless steel material and borosilicate glass are selected as a tool electrode and work material, respectively. Their properties are given in Tables 1 and 2, respectively. A dimensional 50 × 50 × 10-mm graphite block is chosen as an auxiliary counter electrode. To provide a voltage between the cathode and anode, a pulsed DC power supply was used. The experiments were performed with the NaOH electrolyte solution.

2.2 Measurement techniques

The experiments were performed on the UAECDM facility to drill holes in the borosilicate glass. MRR and TEW were taken as response outcomes. To calculate the MRR, the initial and final weight were measured with high-precision weighing machine after T_m machining time. To calculate the MRR, the formula used is expressed in Eq. 1.

$$\mathrm{MRR} = \left\{ \frac{W_i - W_f}{T_m} \right\} \tag{1}$$

where W_i is the initial weight and W_f is the final weight after machining and T_m is the machining time.

The tool electrode schematics before and after machining are shown in Fig. 6. The TEW is measured in terms of volumetric wear and the formula used, as expressed in Eq. 2.

$$\text{Total volumetric TEW} = \frac{\pi h(r_1 - r_2)(-11{r_1}^2 + 2r_1r_2 + 3{r_2}^2)}{6(8r_1 - 5r_2)} + \left(\pi {r_2}^2\right) \times \Delta L \tag{2}$$

where r_1 is tool electrode radius after machining, r_2 is tool electrode radius before machining at the tool electrode bottom surface, ΔL is the longitudinal tool wear, and h is the height of

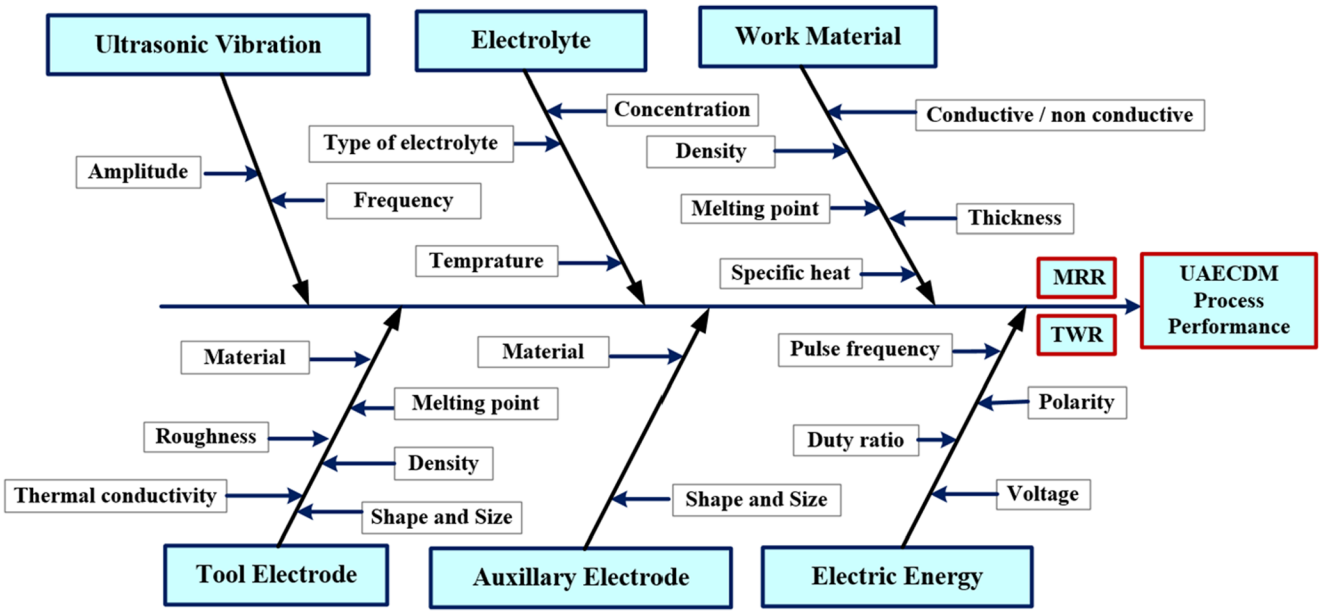

Fig. 5 Ishikawa diagram for MRR and TEW

Table 1 Work material properties

Properties	Unit	Value
Thermal expansion coefficient (ISO 7991)	cm/cm/°K	3.3×10^{-6}
Density	g/cm^3	2.23
Lower annealing temperature	°C	510
Upper annealing temperature	°C	560

the tool electrode edge. A tool maker's microscope (Make: Nikon MM 400, least count of 1 μm) was used to measure the longitudinal tool wear length. A digital stereo zoom microscope was used to capture the tool image.

3 Mathematical modeling for output response

The model was mechanistic in the sense that parameters can be experimentally measured for work material from a few experiments and then used for HOC, MRR, and TEW prediction over different process parameters for wide range. Using the UAECDM process, it was used for drilling in borosilicate glass, where good predictions were obtained at a time using different parameter estimation. The study reported the effects of five process parameters (tool material properties, working material properties, power rating, duty cycle, and applied voltage). Table 3 shows different parameters of input and response outcome used in the experimental study, and Tables 1 and 2 show the properties of borosilicate glass and tool material, respectively. The relationships have been analyzed, taking into account the interaction between these variables. In the case of the ECDM process, the literature reveals various modeling techniques used to establish relationships between input and output. The following assumptions are made using the Buckingham's π theorem for the UAECDM process while developing the mathematical model (Table 4):

- Ultrasonic vibration frequency has been fixed throughout the experiment and is in the range of 26 ± 1 kHz.
- Throughout the experiment, the feed force is also considered constant.
- The properties of workpiece material were taken as homogeneous and isotropic.
- During the experiments, the atmospheric condition remains constant.
- The electrolyte level is assumed to be constant during the experiment.

Table 2 Properties of tool electrode (stainless steel)

Property	Unit	Value
Specific heat (σ)	J/kg K	510
Hardness	HRA	54
Density (ρ)	kg m^{-3}	8030
Linear expansion coefficient (α)	K^{-1}	4.5 × 10–6
Melting point	°C	1426
Thermal conductivity λ	Wm^{-1} K^{-1}	26

In the present article, the dimensional analysis is used to develop the relationship between controlling machining parameters and MRR, HOC, and TEW. The dimensional analysis is based on the Buckingham's π theorem. The dimensional analysis has proved to be a successful approach to the generation of analytical equations with a number of variables [35]. The dimensional analysis is now the theory by which the effect of variables can be lowered through some physical equations [36]. According to the theorem, the system with "n" quantities having "m" fundamental dimensions; then, the variables can be organized in independent dimensionless parameters of "n–m". The process parameters related to MRR and TEW for the UAECDM process are given in Tables 5 and 6, respectively, along with their respective dimensional units. The process variables selected in the UAECDM process are applied voltage, power rating, electrolyte concentration, and T_{on}, whereas the working material's specific heat, melting point, and density, and peak current during the process are taken as the constant parameters.

The present system comprises five fundamental dimensions (mass (M), length (L), time (T), charge (Q), and temperature (θ)) and nine variables for characteristics of performance output (MRR). As per the Buckingham π theorem, for the development of a model, there is a requirement to select the non-repeating and repeating variables. The number of variables to repeat should be equal to fundamental dimensions.

Therefore, in the present scenario, the five repeating variables are selected as follows: peak current, specific heat, melting point, density, and T_{on}, while the non-repeating variables are chosen, power rating, applied voltage, electrolytes concentration, and one dependent variable, which may be MRR for different cases.

3.1 Mathematical modeling for predicting MRR (M) during UAECDM process

The process parameters affecting the MRR (A) during the UAECDM process can be expressed in Eq. 3.

$$M = f(V, T_{on}, E_c, P, I, C_s, T_m, \rho) \quad (3)$$

where M is the MRR, T_{on} is a pulse on time, V is the applied voltage, E_c is electrolyte concentration, P is power rating, I is

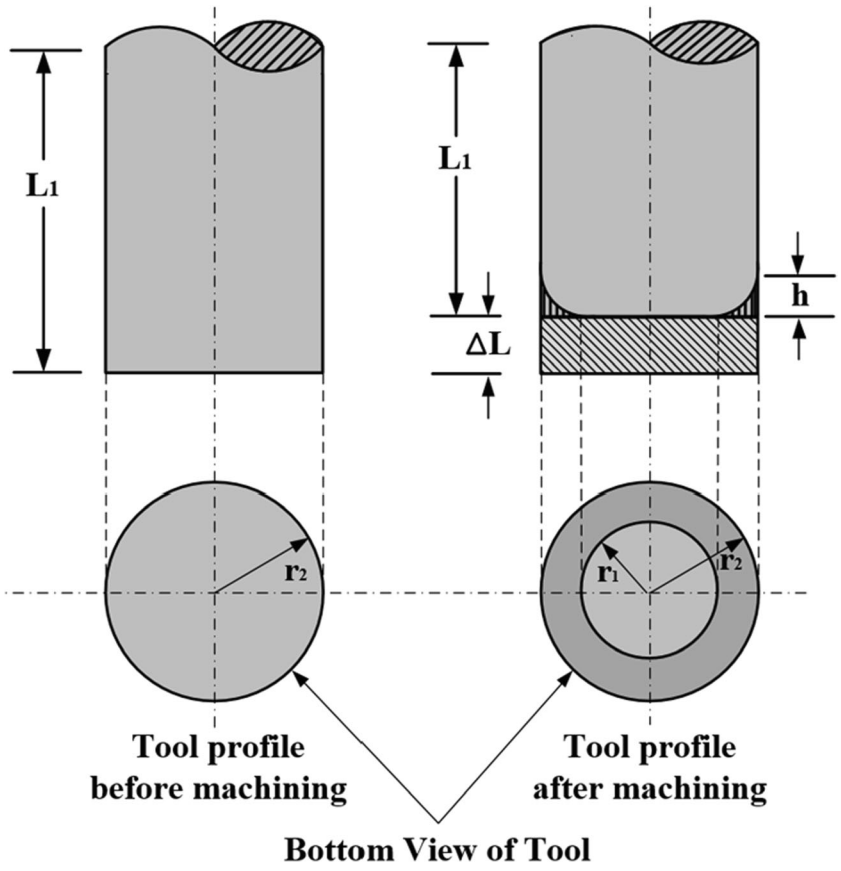

Fig. 6 Schematics of tool electrode before and after machining

peak current, C_s is the specific heat of the work material, T_m is work material's melting point, and ρ is work material's density. The selected non-repeating variables are power rating (P), applied voltage (V), electrolyte concentration (E_c), and material removal rate (M). Process parameters for the groups π_1, π_2, π_3, and π_4 can be expressed as follows:

$$\pi_1 = M\left(I^{a_1}, {C_s}^{b_1}, {T_m}^{c_1}, \rho^{d_1}, {T_{on}}^{e_1}\right) \quad (4)$$

$$\pi_2 = P\left(I^{a_2}, {C_s}^{b_2}, {T_m}^{c_2}, \rho^{d_2}, {T_{on}}^{e_2}\right) \quad (5)$$

$$\pi_3 = V\left(I^{a_3}, {C_s}^{b_3}, {T_m}^{c_3}, \rho^{d_3}, {T_{on}}^{e_3}\right) \quad (6)$$

$$\pi_4 = E_c\left(I^{a_4}, {C_s}^{b_4}, {T_m}^{c_4}, \rho^{d_4}, {T_{on}}^{e_4}\right) \quad (7)$$

where $i = 1, 2, 3$, and 4 are the subscript for Eqs. 4, 5, 6, and 7, respectively. a_i is the exponent of peak current (I), b_i is the exponent of specific heat (C_s), c_i is the exponent of melting point (T_m), d_i is the exponent of work material density (ρ), e_i is the exponent of T_{on}. The ultimate exponent of every fundamental dimension was obtained by substituting each quantity's dimensions and equating to zero since the π are dimensionless groups.

$$\pi_1 = \left(MT^{-1}\right)\left(QT^{-1}\right)^{a_1}\left(L^2T^{-2}\theta^{-1}\right)^{b_1}(\theta)^{c_1}\left(ML^{-3}\right)^{d_1}(T)^{e_1}$$
$$\left(M^0L^0T^0Q^0\theta^0\right) = \left(MT^{-1}\right)\left(QT^{-1}\right)^{a_1}\left(L^2T^{-2}\theta^{-1}\right)^{b_1}(\theta)^{c_1}\left(ML^{-3}\right)^{d_1}(T)^{e_1} \quad (8)$$

Table 3 Input process parameters' and response outcome

Input parameters	Levels					Response outcomes
Electrolyte concentration (%)	10	15	20	25	30	MRR (mg/min)
Pulse on time (T_{on})(ms)	50	66	75	80	83	TEW(mm^3)
Applied voltage (V)	62	66	70	74	78	
Power rating (%)	0	5	10	15	20	
Constants						
Tool	Ø 600-μm solid cylindrical (SS 304)					
Work material	1300-μm-thickness Borosilicate glass					

Table 4 Amplitude produced at the tip of the horn at different power ratings [34]

Power rating (%)	Amplitude (μm)
0	5
5	7
10	8
15	10
20	12
25	14
30	17

Table 5 Process parameters and their dimensional units for UAECDM process

Parameters	Dimensional unit	Unit	Symbol	Values
Variable				
Power rating	ML^2T^{-3}	Watt	P	
Electrolyte concentration	ML^{-3}	kg/m^3	E_c	
Pulse on time	T	Millisecond	T_{on}	
Applied voltage	$ML^2T^{-2}Q^{-1}$	Volt	V	
Constant				
Density	ρ	kg/m^3	ML^{-3}	2230
Specific heat	C_s	J/kg °K	$L^2T^{-2}\theta^{-1}$	800
Melting point	T_m	Kelvin	θ	1093.15
Peak current	I	Ampere	QT^{-1}	3
Response characteristic				
MRR	mg/min	MT^{-1}	M	

Here,
$M: 1 + d_1 = 0,\ L: 2b_1 - 3d_1 = 0,\ T: -1 - a_1 - 2b_1 + e_1 = 0,$
$Q: a_1 = 0,\ \theta: -b_1 + c_1 = 0$

Solving, we get

$$a_1 = 0,\ b_1 = -1.5,\ c_1 = -1.5,\ d_1 = -1,\ e_1 = -2$$

thus

$$\pi_1 = \frac{M}{{C_s}^{1.5}{T_m}^{1.5}\rho{T_{on}}^2} \tag{9}$$

Similarly, we get:

$$\pi_2 = \left(ML^2T^{-3}\right)\left(QT^{-1}\right)^{a_2}\left(L^2T^{-2}\theta^{-1}\right)^{b_2}(\theta)^{c_2}\left(ML^{-3}\right)^{d_2}(T)^{e_2}$$
$$\left(M^0L^0T^0Q^0\theta^0\right) = \left(ML^2T^{-3}\right)\left(QT^{-1}\right)^{a_2}\left(L^2T^{-2}\theta^{-1}\right)^{b_2}(\theta)^{c_2}\left(ML^{-3}\right)^{d_2}(T)^{e_2} \tag{10}$$

$$\pi_2 = \frac{P}{{C_s}^{2.5}{T_m}^{2.5}\rho{T_{on}}^2} \tag{11}$$

$$\pi_3 = \left(ML^2T^{-2}Q^{-1}\right)\left(QT^{-1}\right)^{a_3}\left(L^2T^{-2}\theta^{-1}\right)^{b_3}(\theta)^{c_3}\left(ML^{-3}\right)^{d_3}(T)^{e_3}$$
$$\left(M^0L^0T^0Q^0\theta^0\right) = \left(ML^2T^{-2}Q^{-1}\right)\left(QT^{-1}\right)^{a_3}\left(L^2T^{-2}\theta^{-1}\right)^{b_3}(\theta)^{c_3}\left(ML^{-3}\right)^{d_3}(T)^{e_3} \tag{12}$$

$$\pi_3 = \frac{VI}{{C_s}^{2.5}{T_m}^{2.5}\rho{T_{on}}^2} \tag{13}$$

$$\pi_4 = \left(ML^{-3}\right)\left(QT^{-1}\right)^{a_4}\left(L^2T^{-2}\theta^{-1}\right)^{b_4}(\theta)^{c_4}\left(ML^{-3}\right)^{d_4}(T)^{e_4}$$
$$\left(M^0L^0T^0Q^0\theta^0\right) = \left(ML^{-3}\right)\left(QT^{-1}\right)^{a_4}\left(L^2T^{-2}\theta^{-1}\right)^{b_4}(\theta)^{c_4}\left(ML^{-3}\right)^{d_4}(T)^{e_4} \tag{14}$$

$$\pi_4 = \frac{E_c}{\rho} \tag{15}$$

The dimensionless parameters are obtained for the MRR are as follows:

Table 6 Process parameters and their dimensional units for TEW

Parameters	Dimensional unit	Unit	Symbol	Values
Variables				
Power rating	ML^2T^{-3}	Watt	P	
Pulse on time	T	Millisecond	T_{on}	
Electrolyte concentration	ML^{-3}	kg/m^3	E_c	
Applied voltage	$ML^2T^{-2}Q^{-1}$	Volt	V	
Constant				
Specific heat of the tool	J/kg °K	$L^2T^{-2}\theta^{-1}$	C_{st}	510
Peak current	Ampere	QT^{-1}	I	3
Melting point of the tool	Kelvin	θ	T_{mt}	1699.15
Thermal conductivity of tool	Watt/mK	$MLT^{-3}\theta^{-1}$	k	26
Electrical conductivity of tool	S/m	$M^{-1}L^{-3}T^1Q^2$	σ	1.45×10^6
Density of tool	kg/m^3	ML^{-3}	ρ_t	8030
Response characteristic				
TEW	mm^3	L^3	W	

$\pi_1 = \frac{M}{C_s^{1.5} T_m^{1.5} \rho T_{on}^2}$, $\pi_2 = \frac{P}{C_s^{2.5} T_m^{2.5} \rho T_{on}^2}$, $\pi_3 = \frac{VI}{C_s^{2.5} T_m^{2.5} \rho T_{on}^2}$, $\pi_4 = \frac{E_c}{\rho}$

The final relationship for MRR is assumed as follows:

$$f(\pi_1, \pi_2\ \pi_3, \pi_4) = 0$$

$$\pi_1 = f(\pi_2 \quad \pi_3, \pi_4) \quad \text{or}$$

$$\frac{M}{C_s^{1.5} T_m^{1.5} \rho T_{on}^2} = f\left\{\left(\frac{P}{C_s^{2.5} T_m^{2.5} \rho T_{on}^2}\right)\left(\frac{VI}{C_s^{2.5} T_m^{2.5} \rho T_{on}^2}\right)\left(\frac{E_c}{\rho}\right)\right\}$$

Experimentally, it was found that sonication (tool electrode amplitude) has an important effect on MRR (M) for mathematical equation formulation.

$$M = K\left\{\left(C_s^{1.5} T_m^{1.5} \rho T_{on}^2\right)\left(\frac{P}{C_s^{2.5} T_m^{2.5} \rho T_{on}^2}\right)\left(\frac{VI}{C_s^{2.5} T_m^{2.5} \rho T_{on}^2}\right)\left(\frac{E_c}{\rho}\right)\right\}$$

After rearranging, we get:

$$M = K\left(\frac{PVIE_c}{C_s^{7/2} T_m^{7/2} \rho^2 T_{on}^2}\right) \tag{16}$$

where K is the dimensionless constant

Experiments were performed at the different power rating values to find out the value of K and M. The other process parameters are maintained at a fixed value that has been selected from the literature. The MRR model developed is expressed in Eq. 17, and the results of the experiment show good agreement. The predicted values of MRR were obtained from the developed model, and the average error is found 1.22%, as shown in Table 8.

$$M = \left(-8.98 \times 10^4 P^3 + 1.66 \times 10^6 P^2 + 1.86 \times 10^7 P + 2.73 \times 10^9\right)\left(\frac{VIE_c}{C_s^{7/2} T_m^{7/2} \rho^2 T_{on}^2}\right) \tag{17}$$

Furthermore, the model is developed for MRR at the different values of applied voltage, T_{on}, and electrolyte concentration at the optimal value of the power rating (15%). The results of the experiments are shown in Figs. 6, 7, 8, and 9. Hence, the models for MRR (M) at different values of applied voltage, T_{on}, and electrolyte concentrations are represented in Eqs. 18, 19, and 20, respectively.

$$M = \left(-6.75 \times 10^5 V^3 + 1.19 \times 10^8 V^2 - 6.43 \times 10^9 V + 1.21 \times 10^{11}\right)\left(\frac{PIE_c}{C_s^{7/2} T_m^{7/2} \rho^2 T_{on}^2}\right) \tag{18}$$

$$M = \left(-1.33 \times 10^5 E_c^3 + 3.3 \times 10^6 E_c^2 + 4.99 \times 10^7 E_c + 4.52 \times 10^9\right)\left(\frac{PIV}{C_s^{7/2} T_m^{7/2} \rho^2 T_{on}^2}\right) \tag{19}$$

$$M = \left(5.99 \times 10^6 T_{on}^3 - 8.95 \times 10^7 T_{on}^2 + 4.2 \times 10^8 T_{on} + 2.07 \times 10^9\right)\left(\frac{PIVE_c}{C_s^{7/2} T_m^{7/2} \rho^2}\right) \tag{20}$$

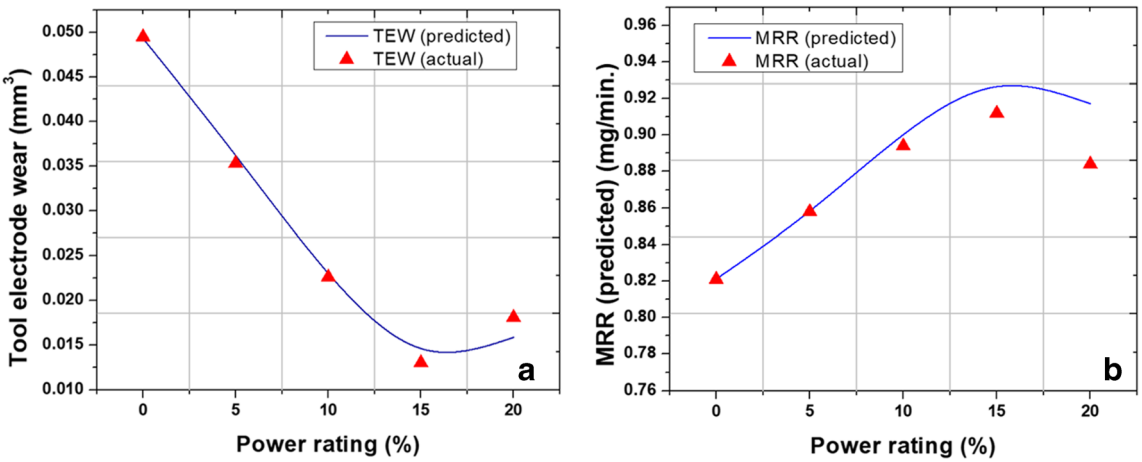

Fig. 7 Relation between power rating with **a** TEW and **b** MRR

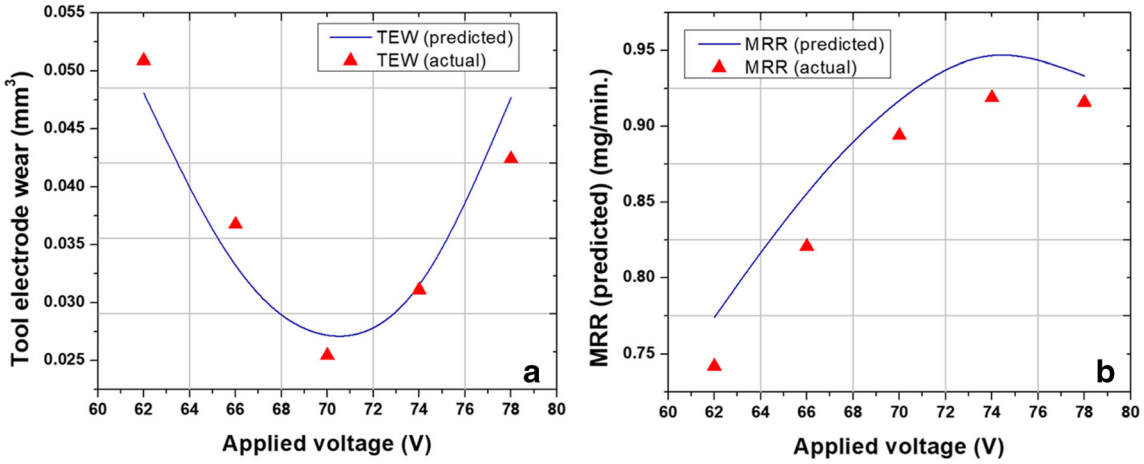

Fig. 8 Relation between applied voltage with **a** TEW and **b** MRR

These equations are in agreement with the results of the experiment, as shown in Table 8. The average error from the developed model between actual MRR and predicted MRR is 3.21%, 3.27%, and 0.41%, respectively, at different values of applied voltage, T_{on}, and electrolyte concentration.

3.2 Mathematical modeling for predicting TEW (*W*) during UAECDM process

The different process parameters associated with TEW during the UAECDM process is expressed in Eq. 21:

$$W = f(V, T_{on}, E_c, P, I, C_{st}, T_{mt}, k, \sigma, \rho_t) \tag{21}$$

where W is the TEW, T_{on}, is a pulse on time; V is the applied voltage; E_c is electrolyte concentration; P is power rating; I is peak current; C_{st} is tool material's specific heat; T_{mt} is tool material's melting point; k is tool electrode's thermal conductivity; σ is tool electrode's electrical conductivity; and ρ_t is the density of the tool material. Expression 21 has 11 variables so that six dimensionless groups formed to predict the TEW during the process. The six non-repeating selected variables are power rating (P), pulse on time (T_{on}), applied voltage (V), electrolyte concentration (E_c), thermal conductivity of the tool material (σ), and tool electrode wear (W). Process parameters for the dimensionless groups π_1, π_2, π_3, π_4, π_5, and π_6 can be expressed as follows:

$$\pi_1 = W\left(I^{a_1}, {C_{st}}^{b_1}, {T_{mt}}^{c_1}, {\rho_t}^{d_1}, \sigma^{e_1}\right) \tag{22}$$

$$\pi_2 = P\left(I^{a_2}, {C_{st}}^{b_2}, {T_{mt}}^{c_2}, {\rho_t}^{d_2}, \sigma^{e_2}\right) \tag{23}$$

$$\pi_3 = V\left(I^{a_3}, {C_{st}}^{b_3}, {T_{mt}}^{c_3}, {\rho_t}^{d_3}, \sigma^{e_3}\right) \tag{24}$$

$$\pi_4 = E_c\left(I^{a_4}, {C_{st}}^{b_4}, {T_{mt}}^{c_4}, {\rho_t}^{d_4}, \sigma^{e_4}\right) \tag{25}$$

$$\pi_5 = T_{on}\left(I^{a_5}, {C_{st}}^{b_5}, {T_{mt}}^{c_5}, {\rho_t}^{d_5}, \sigma^{e_5}\right) \tag{26}$$

$$\pi_6 = k\left(I^{a_6}, {C_{st}}^{b_6}, {T_{mt}}^{c_6}, {\rho_t}^{d_6}, \sigma^{e_6}\right) \tag{27}$$

where $i = 1, 2, 3, 4, 5$, and 6 are the subscript for Eqs. 22, 23, 24, 25, 26, and 27, respectively. a_i is the exponent of peak

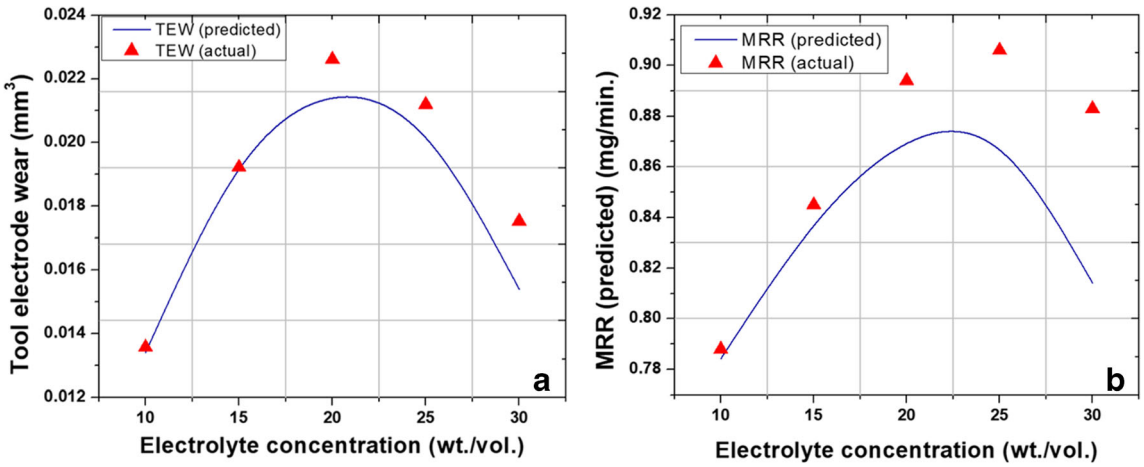

Fig. 9 Relation between electrolyte concentrations with **a** TEW and **b** MRR

current (I), b_i is the exponent of specific heat (C_{st}), c_i is the exponent of melting point (T_{mt}), d_i is the exponent of work material density (ρ_t), e_i is the exponent of T_{on}. The ultimate exponent of every fundamental dimension was obtained by substituting each quantity's dimensions and equating to zero since the π are dimensionless groups.

$$\begin{aligned}\pi_1 &= \left(L^3\right)\left(QT^{-1}\right)^{a_1}\left(L^2T^{-2}\theta^{-1}\right)^{b_1}(\theta)^{c_1}\left(ML^{-3}\right)^{d_1}\left(M^{-1}L^{-3}T^1Q^2\right)^{e_1}\\ \left(M^0L^0T^0Q^0\theta^0\right) &= \left(L^3\right)\left(QT^{-1}\right)^{a_1}\left(L^2T^{-2}\theta^{-1}\right)^{b_1}(\theta)^{c_1}\left(ML^{-3}\right)^{d_1}\left(M^{-1}L^{-3}T^1Q^2\right)^{e_1}\end{aligned} \tag{28}$$

Here,
$M: d_1 - e_1 = 0$, $L: 3 + 2b_1 - 3d_1 - 3e_1 = 0$, $T: -a_1 - 2b_1 + e_1 = 0$, $Q: a_1 + 2e_1 = 0$, $\theta: -b_1 + c_1 = 0$

Solving, we get
$a_1 = -2$, $b_1 = 1.5$, $c_1 = 1.5$, $d_1 = 1$, $e_1 = 1$

Thus,

$$\pi_1 = \frac{{C_{st}}^{1.5} W {T_{mt}}^{1.5}}{I^2 \rho_t \sigma} \tag{29}$$

Similarly, we get:

$$\begin{aligned}\pi_2 &= \left(ML^2T^{-3}\right)\left(QT^{-1}\right)^{a_2}\left(L^2T^{-2}\theta^{-1}\right)^{b_2}(\theta)^{c_2}\left(ML^{-3}\right)^{d_2}\left(M^{-1}L^{-3}T^1Q^2\right)^{e_2}\\ \left(M^0L^0T^0Q^0\theta^0\right) &= \left(ML^2T^{-3}\right)\left(QT^{-1}\right)^{a_2}\left(L^2T^{-2}\theta^{-1}\right)^{b_2}(\theta)^{c_2}\left(ML^{-3}\right)^{d_2}\left(M^{-1}L^{-3}T^1Q^2\right)^{e_2}\end{aligned} \tag{30}$$

$$\pi_2 = \frac{P}{I^{1.333}\, {C_{st}}^{0.5} {T_{mt}}^{0.5} {\rho_t}^{0.333} \sigma^{0.6667}} \tag{31}$$

$$\begin{aligned}\pi_3 &= \left(ML^2T^{-2}Q^{-1}\right)\left(QT^{-1}\right)^{a_3}\left(L^2T^{-2}\theta^{-1}\right)^{b_3}(\theta)^{c_3}\left(ML^{-3}\right)^{d_3}\left(M^{-1}L^{-3}T^1Q^2\right)^{e_3}\\ \left(M^0L^0T^0Q^0\theta^0\right) &= \left(ML^2T^{-2}Q^{-1}\right)\left(QT^{-1}\right)^{a_3}\left(L^2T^{-2}\theta^{-1}\right)^{b_3}(\theta)^{c_3}\left(ML^{-3}\right)^{d_3}\left(M^{-1}L^{-3}T^1Q^2\right)^{e_3}\\ \pi_3 &= \frac{V\sigma^{0.667}}{I^{0.333} {C_{st}}^{0.5} {T_{mt}}^{0.5} {\rho_t}^{0.333}}\end{aligned} \tag{32}$$

$$\begin{aligned}\pi_4 &= \left(ML^{-3}\right)\left(QT^{-1}\right)^{a_4}\left(L^2T^{-2}\theta^{-1}\right)^{b_4}(\theta)^{c_4}\left(ML^{-3}\right)^{d_4}\left(M^{-1}L^{-3}T^1Q^2\right)^{e_4}\\ \left(M^0L^0T^0Q^0\theta^0\right) &= \left(ML^{-3}\right)\left(QT^{-1}\right)^{a_4}\left(L^2T^{-2}\theta^{-1}\right)^{b_4}(\theta)^{c_4}\left(ML^{-3}\right)^{d_4}\left(M^{-1}L^{-3}T^1Q^2\right)^{e_4}\end{aligned} \tag{33}$$

$$\pi_4 = \frac{E_c}{\rho_t} \tag{34}$$

$$\begin{aligned}\pi_5 &= (T)\left(QT^{-1}\right)^{a_5}\left(L^2T^{-2}\theta^{-1}\right)^{b_5}(\theta)^{c_5}\left(ML^{-3}\right)^{d_5}\left(M^{-1}L^{-3}T^1Q^2\right)^{e_5}\\ \left(M^0L^0T^0Q^0\theta^0\right) &= (T)\left(QT^{-1}\right)^{a_5}\left(L^2T^{-2}\theta^{-1}\right)^{b_5}(\theta)^{c_5}\left(ML^{-3}\right)^{d_5}\left(M^{-1}L^{-3}T^1Q^2\right)^{e_5}\end{aligned} \tag{35}$$

$$\pi_5 = \frac{T_{on} C_{st} T_{mt} {\rho_t}^{0.333} \sigma^{0.333}}{I^{0.6667}} \tag{36}$$

$$\begin{aligned}\pi_6 &= \left(MLT^{-3}\theta^{-1}\right)\left(QT^{-1}\right)^{a_6}\left(L^2T^{-2}\theta^{-1}\right)^{b_6}(\theta)^{c_6}\left(ML^{-3}\right)^{d_6}\left(M^{-1}L^{-3}T^1Q^2\right)^{e_6}\\ \left(M^0L^0T^0Q^0\theta^0\right) &= \left(MLT^{-3}\theta^{-1}\right)\left(QT^{-1}\right)^{a_6}\left(L^2T^{-2}\theta^{-1}\right)^{b_6}(\theta)^{c_6}\left(ML^{-3}\right)^{d_6}\left(M^{-1}L^{-3}T^1Q^2\right)^{e_6}\end{aligned} \tag{37}$$

$$\pi_6 = \frac{k\sigma^{0.333}}{I^{0.6667} C_{st} {\rho_t}^{0.6667}} \tag{38}$$

The dimensionless parameters are obtained for the TEW are as follows:

$$\pi_1 = \frac{C_{st}^{1.5} W T_{mt}^{1.5}}{I^2 \rho_t \sigma}, \pi_2 = \frac{P}{I^{1.333}\, C_{st}^{0.5} T_{mt}^{0.5} \rho_t^{0.333} \sigma^{0.6667}}, \pi_3 = \frac{V \sigma^{0.667}}{I^{0.333} C_{st}^{0.5} T_{mt}^{0.5} \rho_t^{0.333}}, \pi_4 = \frac{E_c}{\rho_t}\pi_5 = \frac{T_{on} C_{st} T_{mt} \rho_t^{0.333} \sigma^{0.333}}{I^{0.6667}}, \pi_6 = \frac{k\sigma^{0.333}}{I^{0.6667} C_{st} \rho_t^{0.6667}}$$

The final relationship for TEW is assumed as follows:

$$f(\pi_1, \pi_2\, \pi_3, \pi_4, \pi_5, \pi_6) = 0$$

$$\pi_1 = f(\pi_2\, \pi_3, \pi_4, \pi_5, \pi_6)$$

$$\frac{C_{st}^{1.5} W T_{mt}^{1.5}}{I^2 \rho_t \sigma} = f\left\{ \left(\frac{P}{I^{1.333}\, C_{st}^{0.5} T_{mt}^{0.5} \rho_t^{0.333} \sigma^{0.6667}}\right)\left(\frac{V\sigma^{0.667}}{I^{0.333} C_{st}^{0.5} T_{mt}^{0.5} \rho_t^{0.333}}\right)\left(\frac{E_c}{\rho}\right)\left(\frac{T_{on} C_{st} T_{mt} \rho_t^{0.333} \sigma^{0.333}}{I^{0.6667}}\right)\left(\frac{k\sigma^{0.333}}{I^{0.6667} C_{st} \rho_t^{0.6667}}\right)\right\}$$

After rearranging, we get:

$$W = \mathrm{K}\left(\frac{PVE_c k\sigma^{5/3} T_{on}}{I \rho_t C_{st}^{5/2} T_{mt}^{3/2}}\right) \tag{39}$$

Experiments were performed at the different power rating values to find out the value of K and W. The other process parameters are maintained at a fixed value that has been selected from the literature. The TEW model developed is expressed in Eq. 40, and the results of the experiment show good agreement. The predicted values of TEW were obtained from the developed model, and the average error is found 1.48%, as shown in Table 7.

$$W = \left(3.23 \times 10^{-10} P^3 - 3.58 \times 10^{-9} P^2 - 7.89 \times 10^{-8} P + 1.77 \times 10^{-6}\right)\left(\frac{VE_c k\sigma^{5/3} T_{on}}{I \rho_t C_{st}^{5/2} T_{mt}^{3/2}}\right) \tag{40}$$

Further, the model is developed for TEW at the different values of T_{on}, applied voltage, and electrolyte concentration at the optimal value of the power rating (15%). The results of the experiments are shown in Figs. 7, 8, 9, and 10. Hence, the models for TEW (W) at different values of applied voltage, electrolyte concentration, and T_{on} are represented in Eqs. 16, 17, and 18, respectively.

$$W = \left(1 \times 10^{-9} V^3 - 1.25 \times 10^{-7} V^2 + 2.74 \times 10^{-6} V + 7.6 \times 10^{-5}\right)\left(\frac{PE_c k\sigma^{5/3} T_{on}}{I \rho_t C_{st}^{5/2} T_{mt}^{3/2}}\right) \tag{41}$$

$$W = \left(2.87 \times 10^{-23} E_c^3 - 5.02 \times 10^{-9} E_c^2 + 2.08 \times 10^{-7} E_c - 6.17 \times 10^{-7}\right)\left(\frac{PVk\sigma^{5/3} T_{on}}{I \rho_t C_{st}^{5/2} T_{mt}^{3/2}}\right) \tag{42}$$

$$W = \left(-7.53 \times 10^{-9} T_{on}^3 + 4.62 \times 10^{-8} T_{on}^2 - 9.68 \times 10^{-9} T_{on} + 7.85 \times 10^{-8}\right)\left(\frac{PVE_c k\sigma^{5/3}}{I \rho_t C_{st}^{5/2} T_{mt}^{3/2}}\right) \tag{43}$$

Table 7 Comparison of TEW with experimental and predicted results

S. no.	Applied voltage (V)	Power rating (%)	Electrolyte conc. (wt./vol.)	Pulse on time (ms)	Actual TEW (mm^3)	Predicted TEW (mm^3)	Average error (%)
1	62	10	20	3	0.0508	0.0480	1.10
2	66	10	20	3	0.0367	0.0332	
3	70	10	20	3	0.0254	0.0271	
4	74	10	20	3	0.0310	0.0315	
5	78	10	20	3	0.0424	0.0476	
6	70	0	20	3	0.0494	0.0493	1.48
7	70	5	20	3	0.0353	0.0362	
8	70	10	20	3	0.0254	0.0230	
9	70	15	20	3	0.0130	0.0146	
10	70	20	20	3	0.0180	0.0158	
11	70	10	10	3	0.0135	0.0134	6.92
12	70	10	15	3	0.0192	0.0191	
13	70	10	20	3	0.0254	0.0214	
14	70	10	25	3	0.0212	0.0201	
15	70	10	30	3	0.0175	0.0154	
16	70	10	20	1	0.0098	000.01	1.69
17	70	10	20	2	0.0169	0.0171	
18	70	10	20	3	0.0254	0.0244	
19	70	10	20	4	0.0268	0.0277	
20	70	10	20	5	0.0212	0.0228	

These TEW models are validated with the experimental results with the stainless steel tool electrode, and these models also stand for other materials. The universal models are developed for the TEW and are in line with the results reported [32]. These equations have good agreement with the results of the experiment, as shown in Table 7. The average error between actual TEW and predicted TEW is 1.1%, 6.92%, and 1.69%, respectively, at different values of T_{on}, applied voltage, and electrolyte concentration. Those models can be further used during the UAECDM process for further investigations on TEW.

4 Results and discussion

For drilling holes in borosilicate glass using the UAECDM process, the MRR and TEW were taken as output responses. The various material properties (melting point, specific heat, and thermal conductivity) are an essential aspect of material removal during the UAECDM process. The temperature generated at the machining zone should be above the melting point. The amount of thermal energy required to raise the temperature in the machining zone is associated with specific

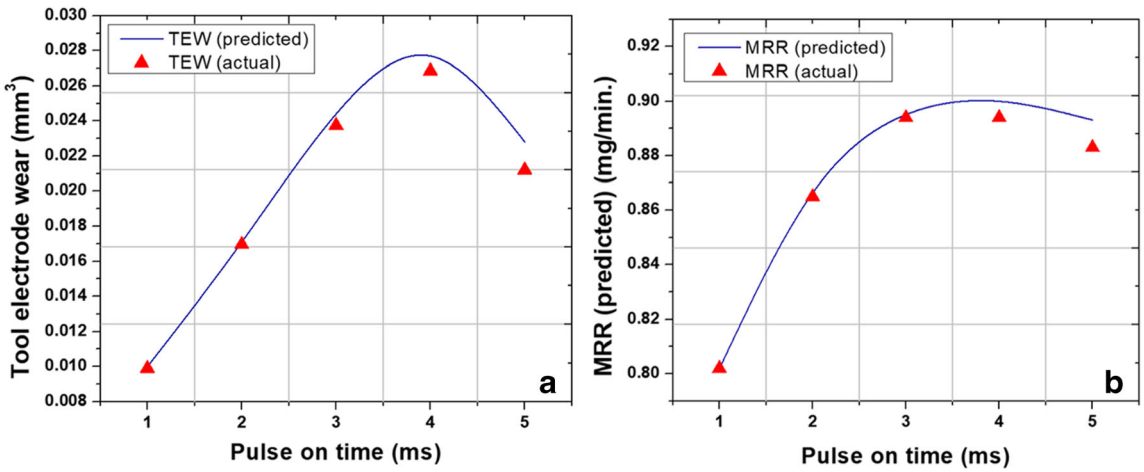

Fig. 10 Relation between pulse on time with **a** TEW and **b** MRR

heat. The thermal conductivity of work material and the tool electrode affects the heat transfer rate. The performance characteristics are discussed using experimental and predicted results. Table 3 shows the process parameters selected for the experiments. The following section addresses the outcomes and discussion.

4.1 Effect of power rating on TEW and MRR

The tool electrode often gets worn out at higher thermal energy in the machining zone along with material removal from the work material. Therefore, TEW and MRR are considered output responses. Figure 7 shows the effect of power rating on the TEW and MRR. Figure 7a and b show that there is a decrease in TEW and a rise in the MRR, up to a power rating of 15%. At the same time, the other parameters are maintained at a fixed value (T_{on}: 3 ms, applied voltage: 70 V, electrolyte concentration: 20% wt./vol.). Because of the reduction in the departure radius of the gas bubble with an increase in the amplitude of ultrasonic vibrations, the thickness of the gas film decreases. The thinner gas film produces low-intensity and high-frequency discharges, which decreases TEW and increases MRR because the discharge energy is channelized beneath the tool electrode. The discharge intensity decreases with the reduction in the gas film thickness. The thermal conductivity of the tool electrode is higher than the work material that transfers the heat from the machining zone to the environment or electrolyte, resulting in the decrease in the TEW with an increase in power rating. But the melting point of the work material is lower than the tool electrode; hence, the MRR does not affect by the reduction in thermal energy in the machining zone. However, with an improvement in the frequency of discharges, the MRR improves with the improved quality of the drilled microholes. The predicted results and experimental results reflect similar TEW and MRR trends, as shown in Fig. 7a, b. Tables 7 and 8 give the actual and predicted TEW and MRR values from experiments and mathematical models. The average error was found to be 1.48% and 1.22%, respectively, between actual and predicted values for TEW and MRR.

4.2 Effect of applied voltage on TEW and MRR

In the UAECDM process, the applied voltage is an essential parameter, and it defines the amount of discharge energy produced in the working gap. Figure 8 shows the relation of TEW and MRR with applied voltage. It was observed that TEW decreases up to 70 V applied voltage; beyond that, it starts increasing. With an increase in applied voltage, the thickness of the gas film increases, generating high-intensity discharges in the working gap. The higher thermal energy melts the sodium and silicon in the machining zone; these molten material combines and forms a sodium silicate compound [11]. The

Table 8 Comparison of MRR with experimental and predicted results

S. no.	Applied voltage (V)	Power rating (%)	Electrolyte conc. (wt./vol.)	Pulse on time (ms)	Predicted MRR (mg/min)	Actual MRR (mg/min)	Average error (%)
1	62	10	20	3	0.774	0.742	3.21
2	66	10	20	3	0.855	0.821	
3	70	10	20	3	0.917	0.894	
4	74	10	20	3	0.946	0.919	
5	78	10	20	3	0.933	0.916	
6	70	0	20	3	0.821	0.821	1.22
7	70	5	20	3	0.858	0.858	
8	70	10	20	3	0.900	0.894	
9	70	15	20	3	0.926	0.912	
10	70	20	20	3	0.917	0.884	
11	70	10	10	3	0.784	0.788	3.27
12	70	10	15	3	0.836	0.845	
13	70	10	20	3	0.869	0.894	
14	70	10	25	3	0.866	0.906	
15	70	10	30	3	0.814	0.883	
16	70	10	20	1	0.801	0.802	0.41
17	70	10	20	2	0.866	0.865	
18	70	10	20	3	0.895	0.894	
19	70	10	20	4	0.9	0.891	
20	70	10	20	5	0.893	0.883	

sodium silicate coating is an insulating material that is deposited over the tooltip that decreases the thermal conductivity at the tooltip. The deposition coating of the molten glass and sodium on the tool electrode reduces the TEW at a high temperature can be seen from Fig. 8.

The generated thermal energy in the machining zone increases with an increase in applied voltage. The temperature rise in the machining zone is above the recrystallization temperature and results in a further rise in the TEW. At the same time, high discharges increase the MRR up to 74-V applied voltage. The increase in MRR is due to both the increase in depth of penetration as well as the hole over cut. But at higher applied voltage, the availability of electrolytes in the machining zone decreases, causing intermittent discharges and consequently decreases in the TEW and MRR, as shown in Fig. 8a, b. The results obtained for TEW and MRR from experiments have a good agreement with the mathematical models (Eqs. 41 and 18), as shown in Fig. 8a, b. The actual and predicted values from experiments and mathematical models of TEW and MRR are given in Tables 7 and 8. It was found that the average error for TEW and MRR between actual and predicted values are 1.1% and 3.21%, respectively.

4.3 Effect of electrolyte concentration on TEW and MRR

An essential component in the UAECDM process is the electrochemical cell, where electrolyte (NaOH) is the prime element. During electrolysis, it provides the conductive path to the H^+ and OH^- ions. Consequently, the H^+ ions combine and form hydrogen gas bubbles at the tool electrode. The gas film around the tool electrode is formed because of the coalescing of these accumulated hydrogen gas bubbles. Electrolytes concentration is an influential parameter that governs the formation of gas films during the process. Figure 9 shows the relationship between electrolyte concentration and TEW and MRR. The TEW and MRR increase with an increase in the electrolyte concentration, as shown in Fig. 9. Since the specific conductance rises with an increase in the electrolytes concentration. The hydrogen gas bubble generation increases at high conductance, which enhances the frequency of film formation. Consequently, high-frequency discharges generate, enhancing the thermal energy in the machining zone, and contribute to an increase in MRR and TEW. The electrical conductance and gas bubble departure radius decrease at higher electrolyte concentrations, resulting in the evolution of small-sized gas bubbles. Therefore, thin gas film formation takes place, which reduces the intensity of discharges and reduces the TEW and MRR, as shown in Fig. 9. Figure 9 a and b shows the TEW and MRR obtained through experiments following similar trends as the mathematical models (Eqs. 42 and 19). The actual and predicted values of TEW and MRR from experiments and mathematical models are given in Tables 7 and 8. It was found that the average error for TEW and MRR between actual and predicted is 6.92% and 3.27%, respectively.

4.4 Effect of pulse on time (T_{on}) on TEW and MRR

During the UAECDM process, the T_{on} attributes the duration of the input energy. Longer T_{on} leads to an increase in thermal energy at the machining zone, which evaporates the electrolyte solution and results in the formation of an inconsistent and unstable gas film. Henceforth, the performance characteristics of the UAECDM process deteriorates. Figure 10 shows the relation between TEW and MRR with T_{on} during the UAECDM process. The other process parameters are maintained at a fixed value (power rating: 15%, applied voltage: 70 V, electrolyte concentration: 20% wt./vol.). From Fig. 10, it is observed that TEW and MRR increase up to 4 ms T_{on}, after which the trend is reversed. The TEW increases as the T_{on} increases from 1 to 4 ms, due to the high thermal energy available at the tooltip. At higher thermal energy in the machining zone, the tool material is heated beyond the recrystallization temperature, which results in an increase in TEW. But higher thermal energy in the machining zone increases the MRR due to the melting and evaporation of the work material.

High thermal energy reduces the stability of the gas film due to the evaporation of electrolyte in the machining zone. Gas film formation is inconsistent due to the lack of electrolytes, which reduces the amount of thermal energy in the machining zone, resulting in decreases in the MRR when the T_{on} is above the optimum value. Tables 7 and 8 list the modeling and experimental results. They indicate that the expected results match the results of the experiments. The average error for TEW and MRR between the actual and the predicted value is 1.69% and 0.41%, respectively.

5 Conclusions

In the present investigation, an indigenous experimental ECDM facility for machining borosilicate glass was developed. The critical influencing parameters like power rating, T_{on}; applied voltage, and electrolyte concentration were identified during the UAECDM process. The effect of sonication has been investigated during the ECDM process. Mathematical models were developed for predicting MRR and TEW using the dimensional analysis during the UAECDM process. Experimental results are validated with the predicted values from the MRR and TEW mathematical models. Following a detailed analysis of the predicted and experimental results for the output performance of the UAECDM process, the main conclusions are drawn as follows:

- The mathematical models developed for the MRR and TEW during the UAECDM process show good agreement with the experiment results. For MRR and TEW, the average error was less than 4% and 7%, respectively.
- During the ECDM process, the introduction of sonication reduces the gas bubble departure radius, which generates stable and thin gas films around the tool and results in the generation of high-frequency and low-intensity discharges, which increases the MRR approx. 12%.
- The TEW for UAECDM has been found to be decreased by 73% at a 15% power rating for stainless steel in comparison with the ECDM process and found to be in line with other materials.

References

1. Kumar J (2013) Ultrasonic machining-a comprehensive review. Mach Sci Technol 17:325–379. https://doi.org/10.1080/10910344.2013.806093
2. Dvivedi A, Kumar P (2007) Surface quality evaluation in ultrasonic drilling through the Taguchi technique. Int J Adv Manuf Technol 34:131–140. https://doi.org/10.1007/s00170-006-0586-3
3. Pujana J, Rivero A, Celaya A, López de Lacalle LN (2009) Analysis of ultrasonic-assisted drilling of Ti6Al4V. Int J Mach Tools Manuf 49:500–508. https://doi.org/10.1016/j.ijmachtools.2008.12.014
4. Ni C, Zhu L, Liu C, Yang Z (2018) Analytical modeling of tool-workpiece contact rate and experimental study in ultrasonic vibration-assisted milling of Ti–6Al–4V. Int J Mech Sci 142–143: 97–111. https://doi.org/10.1016/J.IJMECSCI.2018.04.037
5. Lotfi M, Amini S, Ashrafi H (2019) Theoretical and numerical modeling of tool–chip friction in ultrasonic-assisted turning. Proc Inst Mech Eng Part E J Process Mech Eng 233:824–838. https://doi.org/10.1177/0954408918812271
6. Kremer D, Lebrun JL, Hosari B, Moisan A (1989) Effects of ultrasonic vibrations on the performances in EDM. CIRP Ann - Manuf Technol 38:199–202. https://doi.org/10.1016/S0007-8506(07)62684-5
7. Yue TM, Chan TW, Man HC, Lau WS (1996) Analysis of ultrasonic-aided laser drilling using finite element method. CIRP Ann - Manuf Technol 45:169–172. https://doi.org/10.1016/S0007-8506(07)63040-6
8. Han MS, Min BK, Lee SJ (2008) Modeling gas film formation in electrochemical discharge machining processes using a side-insulated electrode. J Micromech Microeng 18. https://doi.org/10.1088/0960-1317/18/4/045019
9. Singh T, Dvivedi A (2016) Developments in electrochemical discharge machining: a review on electrochemical discharge machining, process variants and their hybrid methods. Int J Mach Tools Manuf 105:1–13. https://doi.org/10.1016/J.IJMACHTOOLS.2016.03.004
10. Singh T, Dvivedi A (2020) On prolongation of discharge regime during ECDM by titrated flow of electrolyte. Int J Adv Manuf Technol 107:1819–1834. https://doi.org/10.1007/s00170-020-05126-y
11. Singh T, Dvivedi A (2018) On performance evaluation of textured tools during micro-channeling with ECDM. J Manuf Process 32: 699–713. https://doi.org/10.1016/j.jmapro.2018.03.033
12. Jain VK, Adhikary S (2008) On the mechanism of material removal in electrochemical spark machining of quartz under different polarity conditions. J Mater Process Technol 200:460–470. https://doi.org/10.1016/J.JMATPROTEC.2007.08.071
13. Arya RK, Dvivedi A (2019) Investigations on quantification and replenishment of vaporized electrolyte during deep micro-holes drilling using pressurized flow-ECDM process. J Mater Process Technol 266:217–229. https://doi.org/10.1016/J.JMATPROTEC.2018.10.035
14. Bhattacharyya B, Doloi B, Sorkhel S (1999) Experimental investigations into electrochemical discharge machining (ECDM) of non-conductive ceramic materials. J Mater Process Technol 95:145–154. https://doi.org/10.1016/S0924-0136(99)00318-0
15. Wüthrich R, Fascio V (2005) Machining of non-conducting materials using electrochemical discharge phenomenon—an overview. Int J Mach Tools Manuf 45:1095–1108. https://doi.org/10.1016/j.ijmachtools.2004.11.011
16. Nguyen KH, Lee PA, Kim BH (2015) Experimental investigation of ECDM for fabricating micro structures of quartz. Int J Precis Eng Manuf 16:5–12. https://doi.org/10.1007/s12541-015-0001-9
17. Elhami S, Razfar MR (2018) Effect of ultrasonic vibration on the single discharge of electrochemical discharge machining. Mater Manuf Process 33:444–451. https://doi.org/10.1080/10426914.2017.1328113
18. Rathore RS, Dvivedi A (2020) Sonication of tool electrode for utilizing high discharge energy during ECDM. Mater Manuf Process 35:415–429. https://doi.org/10.1080/10426914.2020.1718699
19. Sarkar BR, Doloi B, Bhattacharyya B (2006) Parametric analysis on electrochemical discharge machining of silicon nitride ceramics. Int J Adv Manuf Technol 28:873–881. https://doi.org/10.1007/s00170-004-2448-1
20. Kamaraj AB, Jui SK, Cai Z, Sundaram MM (2015) A mathematical model to predict overcut during electrochemical discharge machining. Int J Adv Manuf Technol 81:685–691. https://doi.org/10.1007/s00170-015-7208-x
21. Singh T, Rathore RS, Dvivedi A (2020) Experimental investigations, empirical modeling and multi objective optimization of performance characteristics for ECDD with pressurized feeding method. Measurement 149:107017. https://doi.org/10.1016/J.MEASUREMENT.2019.107017
22. Tsai KM, Wang PJ (2001) Semi-empirical model of surface finish on electrical discharge machining. Int J Mach Tools Manuf 41: 1455–1477. https://doi.org/10.1016/S0890-6955(01)00015-3
23. Kumar J, Khamba JS, Mohapatra SK (2009) Investigating and modeling tool-wear rate in the ultrasonic machining of titanium. Int J Adv Manuf Technol 41:1107–1117. https://doi.org/10.1007/s00170-008-1556-8
24. Patil NG, Brahmankar PK (2010) Determination of material removal rate in wire electro-discharge machining of metal matrix composites using dimensional analysis. Int J Adv Manuf Technol 51:599–610. https://doi.org/10.1007/s00170-010-2633-3
25. Singh R (2014) Modeling of surface hardness in hot chamber die casting using Buckingham's π approach. J Mech Sci Technol 28: 699–704. https://doi.org/10.1007/s12206-013-1133-4
26. Singh S, Singh R (2015) Wear modelling of Al-Al2O3 functionally graded material prepared by FDM assisted investment castings using dimensionless analysis. J Manuf Process 20:507–514. https://doi.org/10.1016/j.jmapro.2015.01.007
27. Bains PS, Sidhu SS, Payal HS (2016) Semi empirical modeling of magnetic field assisted ed machining of metal matrix composites. In: Proceedings of the American Society for Composites - 31st Technical Conference, ASC 2016
28. Goel H, Rath U, Pandey PM (2019) Modelling of MRR and hole taper for ultrasonic assisted jet electrochemical micro-drilling

process using Buckingham's π theorem. Int J Mechatronics Manuf Syst 12:140–162. https://doi.org/10.1504/IJMMS.2019.102949
29. Ravindranatha Reddy P, Jayachandra Reddy G, Prasanthi G (2020) Mathematical modeling of material removal rate using Buckingham pi theorem in electrical discharge machining of Hastelloy C276. Lect Notes Mech Eng:843–852. https://doi.org/10.1007/978-981-15-1201-8_90
30. Phate M, Toney S, Phate V (2020) Modelling and investigating the impact of EDM parameters on surface roughness in EDM of Al / Cu / Ni alloy. Aust J Mech Eng:1–14. https://doi.org/10.1080/14484846.2020.1790478
31. Kanthababu M, Mohankumar V (2020) Semi-empirical model for depth of cut in abrasive waterjet machining of metal matrix composites. J Braz Soc Mech Sci Eng 2. https://doi.org/10.1007/s40430-020-02581-2
32. Ziki JDA, Wüthrich R (2012) Tool wear and tool thermal expansion during micro-machining by spark assisted chemical engraving. Int J Adv Manuf Technol 61:481–486. https://doi.org/10.1007/s00170-011-3731-6
33. Elhami S, Razfar MR (2017) Study of the current signal and material removal during ultrasonic-assisted electrochemical discharge machining. Int J Adv Manuf Technol 92:1591–1599. https://doi.org/10.1007/s00170-017-0224-2
34. Sandeep K, Akshay D (2018) Fabrication of microchannels using rotary tool micro-USM: an experimental investigation on tool wear reduction and form accuracy improvement. J Manuf Process 32:802–815. https://doi.org/10.1016/j.jmapro.2018.04.008
35. Wang J (2007) Predictive depth of jet penetration models for abrasive waterjet cutting of alumina ceramics. Int J Mech Sci 49:306–316. https://doi.org/10.1016/J.IJMECSCI.2006.09.005
36. Anders D, Münker T, Artel J, Weinberg K (2012) A dimensional analysis of front-end bending in plate rolling applications. J Mater Process Technol 212:1387–1398. https://doi.org/10.1016/j.jmatprotec.2012.02.005